

# Collaborative Evaluation of CFD-to-ROM Dynamic Modeling

Mehdi Ghoreyshi<sup>1\*</sup>, Neal T. Frink<sup>2†</sup>, Michel van Rooij<sup>3‡</sup>  
 Andrew J. Lofthouse<sup>1§</sup>, Russell M. Cummings<sup>1¶</sup>, Sudheer Nayani<sup>4||</sup>

<sup>1</sup> *High Performance Computing Research Center, USAF Academy, Colorado 80840*

<sup>2</sup> *NASA Langley Research Center, Hampton, Virginia 23681*

<sup>3</sup> *National Aerospace Laboratory NLR, Amsterdam, The Netherlands*

<sup>4</sup> *Analytical Services & Materials Inc., Hampton, Virginia 23666*

This work presents and discusses findings from a NATO STO collaborative research on the reduced order aerodynamic modeling of a NACA 0012 airfoil and a generic swept wing UCAV. The linear and nonlinear reduced order models are created based on the superposition integrals of the step response with the derivative of its corresponding input signal. Step responses are calculated using CFD and a grid motion approach that allows separating the effects of angle of attack and sideslip angle from angular rates. This approach was previously tested using Cobalt flow solver, however to demonstrate its generalization capability, four different flow solvers are used in this study: Cobalt and Kestrel at United States Air Force Academy (USAF), USM3D at NASA Langley Research Center (LaRC), and ENSOLV at the Netherlands National Aerospace Laboratories (NLR). Step changes in the angle of attack and pitch rate are obtained using these CFD codes. For the UCAV configuration, the lateral step responses to sideslip angle, roll and yaw rates are also calculated. The step predictions of the codes are compared with each other. Aerodynamic models are then created from these step responses and are used to predict responses to arbitrary motions (inputs). The model predictions are compared with CFD (full-order) and available experiments. The results demonstrate that step functions can be easily calculated by CFD codes. Overall, the angle-of-attack and pitch rate responses are very similar for each solver particularly at small angles of attack. Discrepancies at higher angles are probably due to differences in grids and solver numerical algorithms. The step responses show an initial jump as the grid begins to move. The initial jumps become smaller with increasing Mach number. All responses will then asymptotically reach a steady-state value. The results show that much less time is required to reach the steady-state solutions for the UCAV geometry than two-dimensional airfoil. Finally, the model predictions match the CFD data of different motions, all generated within the range of data used for model generation, very well.

\*Senior Aerospace Engineer, Senior Member, AIAA

†Senior Researcher, Configuration Aerodynamics Branch, Research Directorate, MS 499, Associate Fellow, AIAA

‡Computational Aerodynamics

§Director, Senior Member, AIAA

¶Professor of Aeronautics, Associate Fellow, AIAA

||Senior Scientist, Senior Member, AIAA

Distribution A. Approved for Public Release. Distribution unlimited.

## Nomenclature

$A_0$	motion amplitude, rad or deg
$a$	acoustic speed, m/s
$b$	wing span, m
$c$	reference chord, m
$c_{ref}$	reference chord, m
$C_l$	roll moment coefficient, $M_x/q_\infty S b$
$C_{l\beta}$	sideslip angle indicial response of roll moment coefficient, 1/rad
$C_{lp}$	roll-rate indicial response of roll moment coefficient, 1/rad
$C_{lr}$	yaw-rate indicial response of roll moment coefficient, 1/rad
$C_m$	pitch moment coefficient, $M_y/q_\infty S c$
$C_{m\alpha}$	angle-of-attack indicial response of pitch moment coefficient, 1/rad
$C_{mq}$	pitch-rate indicial response of pitch moment coefficient, 1/rad
$C_N$	normal-force coefficient, $N/q_\infty S$
$C_{N\alpha}$	angle-of-attack indicial response of normal force coefficient, 1/rad
$C_{Nq}$	pitch-rate indicial response of normal force coefficient, 1/rad
$C_n$	roll moment coefficient, $M_z/q_\infty S b$
$C_{n\beta}$	sideslip angle indicial response of yaw moment coefficient, 1/rad
$C_{np}$	roll-rate indicial response of yaw moment coefficient, 1/rad
$C_{nr}$	yaw-rate indicial response of yaw moment coefficient, 1/rad
$k$	reduced frequency, $\omega c/2V$
$M_x$	roll moment, N-m
$M_y$	pitch moment, N-m
$M_z$	yaw moment, N-m
$N$	normal force, N
$\bar{p}, \bar{q}, \bar{r}$	pitch, roll, and yaw rates, rad/s
$p$	normalized pitch rate, $\bar{p}b/(2V)$
$q$	normalized pitch rate, $\bar{q}c/(2V)$
$q_\infty$	dynamic pressure, Pa, $\rho V^2/2$
$r$	normalized pitch rate, $\bar{r}b/(2V)$
$Re$	Reynolds number, $\rho V c/\mu$
$S$	Planform area, m <sup>3</sup>
$t^*$	non-dimensional time, $Vt/c$
$t$	time, s
$V$	freestream velocity, m/s
$x, y, z$	aircraft position coordinates

### Greek

$\alpha$	angle of attack, rad
$\dot{\alpha}$	time-rate of change of angle of attack, rad/s
$\beta$	side-slip angle, rad
$\phi$	control surface deflection, rad
$\rho$	air density, kg/m <sup>3</sup>
$\mu$	air viscosity, kg/(m.s)
$\omega$	angular rate, rad/s

## I. Introduction

Accurate modeling of unsteady and nonlinear aerodynamics in flight dynamics and structural analysis still remains a research challenge. Aerodynamic models based on stability derivatives are quasi-steady models and will therefore fail to predict the response of a highly maneuver aircraft at high angles of attack.<sup>1</sup> At these flight conditions, the aerodynamic loads at each time instant depend on the current state as well as

past states of the aircraft (angle of attack, pitch rate, etc.), whereas stability derivative models only depend on the current state. This implies that the predictions from these models will be unchanged regardless of motion frequency or time history. Unsteady experimental data have shown that there is a time lag between quasi-steady model predictions and unsteady flow field measurements.<sup>2</sup> These models can underestimate the actual responses caused by sudden changes in aircraft states as well. The time lag and underestimation of actual airloads may affect the control law design and the stability of structure.

One method of including unsteady effects into aerodynamic predictions is to develop a full-order model (often called a time-marching CFD solution) based on time integration of Navier–Stokes equations.<sup>3,4,5</sup> However, creating a full-order model is a computationally expensive approach and is impractical from a designer’s point of view because it requires a large number of computations for different values of motion frequency and amplitude. An alternative is to use a relatively simple but accurate approximation for the unsteady aerodynamics by using a Reduced Order Model (ROM) that allows describing the unsteady flow in the form of a small number of spatial/temporal modes (typically less than one hundred) compared with the very large number of grid points in the full-order model (on the order of 5 to 50 million or more).<sup>6,7</sup> The ROM can then predict the responses to an arbitrary input much faster than computing the input in a full CFD solution. The ROMs based on step responses are considered in this work.

The convolution of aircraft responses to step inputs is considered as a powerful tool to take into account the time history effects on the aerodynamic coefficients.<sup>8,9,10,11,12</sup> The main challenge in creating these models is estimation of step functions for compressible flow and three-dimensional geometries. The experimental tests are practically nonexistent for step response functions. The analytical solutions are only available for two-dimensional incompressible flow.<sup>13,14</sup> CFD can be considered as an alternative to theory and the experimental measuring of step responses, but special considerations are required to separate the effects of angle-of-attack and pitch-rate from responses or side-slip effects from yaw motions.

Ghoreyshi et al.<sup>15</sup> proposed an approach based on grid motion for CFD-type calculation of step functions. In this approach, the relative velocity between flow and grid is used to simulate a step change in input parameters. One advantage of this method is that the grid motion capability is available in most flow solvers. The earlier methods for calculating response functions such as the small perturbation<sup>16</sup> or surface transpiration approach<sup>17</sup> need access to the solver source codes. Furthermore, these methods have not yet been tested for pitch rate step functions or aircraft configurations.

At USAFA, the grid motion approach was successfully tested to calculate step responses of a number of aircraft configurations using Cobalt flow solver.<sup>15,10,11,12</sup> In Ref. 11, the step responses of SACCON UCAV are calculated with respect to longitudinal and lateral input parameters. A surrogate model with these responses is then used to predict the aerodynamics of the maneuvering SACCON. Ghoreyshi and Cummings<sup>18</sup> used the approach to predict the step responses of T-38 aircraft with respect to control surfaces as well. Again, all these results were obtained with Cobalt flow solver. To demonstrate the generalization capabilities of the grid motion approach for calculating step responses in CFD, the step functions of a close gap NACA 0012 airfoil and SACCON UCAV are calculated with four different CFD flow solvers. The tested codes include Cobalt and Kestrel codes at USAFA, USM3D at LaRC, and ENSOLV at NLR. This work is organized as follows. First the reduced order model is described. The flow solvers are then detailed. Next, the test cases are presented. Finally, the simulation and modeling results will be discussed.

## II. Formulation

### A. Reduced-Order Aerodynamics Modeling

The transient aerodynamic response due to a unit step change in a forcing parameter is a so-called indicial function. Aerodynamic indicial functions can estimate forces and moments induced in any arbitrary maneuver using the well-known Duhamel’s superposition integral.<sup>8</sup> Notice that aerodynamic predictions by using Duhamel’s integral are only valid for linear regimes of flow. To overcome this problem, Tobak<sup>19,9</sup> formulated a nonlinear indicial response model for predicting aerodynamic responses to large amplitude motions.

It is assumed that the time responses in lift due to the step changes in angle of attack,  $\alpha$ , and normalized pitch rate,  $q$ , are denoted as  $C_{L\alpha}$  and  $C_{Lq}$ , respectively. These step changes can be found from a general step input or a unit step (indicial response). The unsteady lift coefficient of small amplitude motions at time

$t$  is obtained as:

$$C_L(t) = C_{L0}(M) + \frac{d}{dt} \left[ \int_0^t C_{L\alpha}(t - \tau, M) \alpha(\tau) d\tau \right] + \frac{d}{dt} \left[ \int_0^t C_{Lq}(t - \tau, M) q(\tau) d\tau \right] \quad (1)$$

where,  $C_{L0}$  denote the zero-angle of attack lift coefficient and is found from static calculations;  $M$  denotes the free-stream Mach number. Equation 1 shows that the lift coefficient at each time  $t$  depends on the states at time  $t$  and the state in previous times after the motion started, i.e.  $t = 0$ .

For a large-amplitude motion, it is assumed that variation of pitch rate responses are small with angle of attack changes. However, the angle-of-attack responses are calculated at different angles of attack and are shown as  $C_{L\alpha}(t - \tau, \alpha, M)$  in the equation.

Likewise, the time responses in pitch moment due to the step changes in  $\alpha$ , and  $q$ , are denoted as  $C_{m\alpha}$  and  $C_{mq}$  and then the pitch moment of large-amplitude motions is estimated as follows:

$$C_m(t) = C_{m0}(M) + \frac{d}{dt} \left[ \int_0^t C_{m\alpha}(t - \tau, \alpha, M) \alpha(\tau) d\tau \right] + \frac{d}{dt} \left[ \int_0^t C_{mq}(t - \tau, M) q(\tau) d\tau \right] \quad (2)$$

Notice that the nonlinear models need more CFD calculations than a linear model. For an aircraft maneuvering in lateral directions, it is assumed that lateral coefficients depend on side-slip angle, roll and yaw rates. The effects of angle of attack and Mach number changes will be included in the sideslip responses to extend the model validity for higher angles of attack. The lateral coefficients are therefore estimated as:

$$C_j(t) = \frac{d}{dt} \left[ \int_0^t C_{j\beta}(t - \tau, \alpha, M) \beta(\tau) d\tau \right] + \frac{d}{dt} \left[ \int_0^t C_{jp}(t - \tau, M) p(\tau) d\tau \right] + \frac{d}{dt} \left[ \int_0^t C_{jr}(t - \tau, M) r(\tau) d\tau \right] \quad (3)$$

where  $C_j = [C_Y, C_l, C_N]$  denotes the coefficients of side force, roll moment, and yaw moment, respectively.  $\beta$  is the side-slip angle;  $p, r$  denote the normalized roll and yaw rates, respectively.

To calculate nonlinear responses of  $C_{L\alpha}(\alpha, M, t)$  and  $C_{m\alpha}(\alpha, M, t)$ , assume a set of angle of attack samples of  $\alpha = [\alpha_1, \alpha_2, \dots, \alpha_n]$  at a free-stream Mach number of  $M$ , where the spacing can be uniform or non-uniform. The response functions at each angle of  $\alpha_i, i = 1, 2, \dots, n$  degrees are then calculated by holding the angle of attack fixed at  $\alpha = \alpha_i$  degrees, and then performing a small step in the angle of attack to  $\alpha = \alpha_i + \Delta\alpha$ . The response functions are then computed by taking the differences between time-varying responses occurring after the step and the steady-state solution at  $\alpha = \alpha_i$  degrees, and dividing them by the magnitude of the step.

To calculate nonlinear responses of  $C_{Y\beta}(\alpha, M, t)$ ,  $C_{l\beta}(\alpha, M, t)$ , and  $C_{n\beta}(\alpha, M, t)$ , again assume a set of angle of attack samples of  $\alpha = [\alpha_1, \alpha_2, \dots, \alpha_n]$  at a free-stream Mach number of  $M$ . The indicial response functions at each angle of  $\alpha_i, i = 1, 2, \dots, n$  degrees are first calculated at zero side-slip angle and by holding the angle of attack fixed at  $\alpha = \alpha_i$  degrees, and then by performing a unit step change in the side-slip angle. The response functions are the differences between time-varying responses occurring after the step and the steady-state solution at zero side-slip angle.

In order to reduce number of samples and therefore the computational cost of models, a special time-dependent surrogate-based modeling approach proposed by Ghoreyshi and Cummings<sup>11</sup> is used. The approach predicts step responses for a new point from available (observed) responses. These observed responses were viewed as a set of time-correlated spatial processes where the output is considered a time-dependent function.

## B. CFD Solvers

Flow solvers of Cobalt, Kestrel, USM3D, and ENSOLV are used in this work. The codes are briefly described below:

### 1. Cobalt

Cobalt<sup>20</sup> solves the unsteady, three-dimensional and compressible Navier-Stokes equations in an inertial reference frame. The ideal gas law and Sutherland's law close the system of equations and the entire equation set is nondimensionalized by free stream density and speed of sound.<sup>20</sup> The Navier-Stokes equations are discretised on arbitrary grid topologies using a cell-centered finite volume method. Second-order accuracy

in space is achieved using the exact Riemann solver of Gottlieb and Groth,<sup>21</sup> and least squares gradient calculations using QR factorization. To accelerate the solution of discretized system, a point-implicit method using analytic first-order inviscid and viscous Jacobians. A Newtonian sub-iteration method is used to improve time accuracy of the point-implicit method. Tomaro et al.<sup>22</sup> converted the code from explicit to implicit, enabling Courant-Friedrichs-Lewy numbers as high as  $10^6$ . Some available turbulence models are the Spalart-Allmaras model,<sup>23</sup> Wilcox's  $k-\omega$  model,<sup>24</sup> and Mentor's SST model.<sup>25</sup>

## 2. USM3D

The NASA computations are performed with TetrUSS/USM3D,<sup>26</sup> which is a parallelized tetrahedral cell-centered, finite volume Navier-Stokes flow solver. The term "cell centered" means that the finite volume flow solution is solved at the centroid of each tetrahedral cell. Inviscid flux quantities are computed across each tetrahedral cell face using various upwind schemes. Spatial discretization is accomplished by a novel reconstruction process, based on an analytical formulation for computing solution gradients within tetrahedral cells. The solution can be advanced in time by a second-order "physical" time step scheme, a second-order "dual" time step scheme, or to a steady-state condition by an implicit backward-Euler scheme. Several turbulence models are available: the Spalart-Allmaras one-equation model, the two-equation  $k-\epsilon$  turbulence model, the Menter Shear Stress Transport (SST) two-equation model, and the nonlinear Algebraic Reynolds Stress Models of Girimaji and Shih/Zhu/Lumley. For generalized grid motion, the USM3D flow solver has been installed as a plug-in to the Fluid Dynamics - Computational Analysis of Dynamically Responsive Environments (FD-CADRE) framework<sup>27</sup> developed at Arnold Engineering Development Center in Tullahoma, Tennessee, US. FD-CADRE is a generalized dynamic process control manager for coupling various plugins, e.g., flow solver, 6-DoF motion generator, aeroelastic structural module, etc. The latest extensions to the USM3D flow solver are recorded in Ref. 28.

## 3. ENSOLV

The NLR's ENSOLV solver<sup>29</sup> is capable of solving the Euler and Navier-Stokes equations on multi-block structured grids for arbitrary configurations. The configuration can be either fixed or moving relative to an inertial reference frame, and can be either rigid or flexible. The equations are nondimensionalized using the free-stream static pressure, the free-stream density, the free-stream temperature and a reference length (for example the reference wing chord). The equations in full conservation form are discretized in space by a second-order accurate, cell-centred, finitevolume method, using multi-block structured grids, central differences, and matrix artificial diffusion. The artificial diffusion consists of a blending of second-order and fourth-order differences with a Jameson-type shock sensor for the basic flow equations and a TVD discontinuity sensor for the turbulence model equations. For steady flow simulations, the discretized time-dependent system of equations is integrated toward the steady-state solution using a five-stage explicit Runge-Kutta scheme. Local-time stepping, implicit residual averaging and multi-grid acceleration techniques are applied.

For time-accurate simulations, the flow solver uses the dual-time stepping scheme, where for each time-step the time-dependent flow equations are integrated in pseudo-time toward a steady-state solution in a similar way as in the steady flow simulation using the same acceleration techniques. Several turbulence models are present in the flow solver ENSOLV, including the Turbulent Non-Turbulent (TNT)  $k-\omega$  model, the EARSM model<sup>30</sup> and a hybrid RANS-LES model for eXtra-Large Eddy Simulation (XLES).<sup>31</sup>

## 4. Kestrel

Kestrel is a relatively new DoD-developed CFD solver in the framework of CREATE<sup>TM</sup> Program which is funded by the High Performance Computing Modernization Program (HPCMP). The CREATE<sup>TM</sup> Program is a 12-year program, started in 2008, and is aimed at addressing the complexity of applying computationally based engineering to improve DoD acquisition processes.<sup>32</sup> CREATE consists of three computationally based engineering tool sets for design of air vehicles, ships, and radio-frequency antennae. The fixed wing analysis code, Kestrel, is part of the Air Vehicles Project (CREATE<sup>TM</sup>-AV) and is a modularized, multidisciplinary, virtual aircraft simulation tool incorporating aerodynamics, structural dynamics, kinematics, and kinetics.<sup>32</sup>

The flow solver component of Kestrel (named kCFD) solves the unsteady, three-dimensional, compressible RANS equations on hybrid unstructured grids.<sup>33</sup> Its foundation is based on Godunov's first-order accurate,

exact Riemann solver.<sup>34</sup> Second-order spatial accuracy is obtained through a least squares reconstruction. The code also uses an implicit Newton sub-iteration method to improve time accuracy as well. Grismer et al<sup>35</sup> parallelized the code, with a demonstrated linear speed-up on thousands of processors. Kestrel receives an eXtensible Markup Language (XML) input file generated by Kestrel User Interface and stores the solution convergence and volume results in a common data structure for later use by the Output Manager component. Some available turbulence models are the Spalart–Allmaras model, SARC, and DDES with SARC.

### C. CFD Calculation of Indicial Functions

The indicial/step functions are directly calculated in CFD codes using a grid motion tool. All considered flow solvers allow translational and rotational degrees of freedom. The grid location is defined by a reference point at each time step. The grid rotation is also defined using the rotation angles of yaw, pitch and roll (bank). The aircraft reference point velocity,  $V_a$ , in an inertial frame is then calculated to achieve the required angles of attack and sideslip, and the forward speed. The velocity is then used to calculate the location. The initial aircraft velocity,  $V_0$ , is specified in terms of Mach number, angle of attack and side-slip angle in the steady-state calculation. The instantaneous aircraft location for the motion file is then defined from the relative velocity vector,  $V_a - V_0$ .

For CFD-type calculation of a step change in angle of attack, the grid immediately starts to move at  $t = 0$  to the right and downward as shown in Fig. 1. The translation continues over time with a constant velocity vector. Since there is no rotation, all the effects in aerodynamic loads are from changes in the angle of attack. For a unit step change in pitch rate, the grid moves and rotates simultaneously. The grid starts to rotate with a unit pitch rate at  $t = 0$ . To hold the angle of attack zero during the rotation, the grid moves right and upward as shown in Fig. 1.

## III. Test Cases

The close gap NACA0012 airfoil and a generic UCAV(Stability And Control CONFIGuration, SACCON) are considered in this work. More details of geometries and computational grids are provided below.

### A. Close Gap NACA0012 Airfoil

Three different grids were generated for CFD simulations of NACA 0012 airfoil in this work. One of grids is unstructured, one is hybrid with prismatic cells on the wall and unstructured elsewhere, and one is fully structured as shown in Figure 2. The pitch axis and the moment reference point are set to  $0.25c$  in all grids, where  $c$  is the airfoil chord.

A quasi-2D grid was constructed for the close gap NACA 0012 airfoil (see Figure 2 (a)) to simulate the static and dynamic motions of the airfoil in the USM3D flow solver. The grid was generated through a special process that is built around the VGRID tetrahedral grid generator.<sup>36</sup> A 2D triangular symmetry-plane grid of 75,986 triangular faces (38,170 nodes) was first generated about the airfoil. This grid was subsequently replicated and translated in the planar normal direction by 0.02 chord lengths, thereby extruding 75,986 prismatic volume elements. Each prism element is then subdivided into 3 tetrahedral elements to produce the final grid of 227,958 cells, with 548 triangular faces around the airfoil surface. The initial spacing from the airfoil surface was prescribed to produce a tetrahedral cell centroid turbulent wall coordinate ( $y+$ ) of 0.5 at a mid-chord distance of  $0.5c$  for a  $Re_c = 4.8$  million. Subsequent USM3D computations confirmed that an average first-cell  $y+ \approx 0.496$  was achieved.

The grid used in ENSOLV solver is structured and shown in Figure 2 (b). This grid was generated using NLR’s in-house domain modeler and grid-generation tools Endomo<sup>37</sup> and Engrid.<sup>38</sup> It is a multi-block C-type grid consisting of a total of 54,272 cells, with 96 cells placed along the chord. The  $y+ \approx 1$  was achieved at  $M = 0.6$ .

An unstructured grid was also generated around NACA 0012 airfoil to perform CFD simulations in Cobalt and Kestrel flow solvers. The computational domain of this grid is rectangular with the airfoil geometry centrally located. The minimal distance from the body to each of the outer boundaries is  $20c$ , where  $c$  is the airfoil chord which is one meter. No-slip, adiabatic wall boundary conditions are employed at the body surface and modified Riemann-invariant conditions were implemented at the far-field boundary. The grid consists of prisms and tetrahedra and was generated using SolidMesh 2D. The overview of the grid is shown in Figure 2 (c). Kestrel simulations reported an average first-cell  $y+ \approx 0.867$  at  $M = 0.6$ .

## B. SACCON UCAV

The SACCON geometry is shown in Fig. 3. The geometry was designed and tested within NATO RTO Task Group AVT-161 (Assessment of Stability and Control prediction Methods for NATO Air and Sea Vehicles).<sup>39</sup> SACCON is a lambda wing planform with a leading edge sweep angle of  $53^\circ$ . The root chord is approximately  $1m$ , the wing span is  $1.53m$ , the reference chord is  $0.48m$ , and the reference area is  $0.77m^2$ . The main sections of the model are the fuselage, the wing section, and wing tip. The configuration is defined by three different profiles at the root section of the fuselage, two sections with the same profile at the inner wing, forming the transition from the fuselage to wing and the outer wing section. Finally, the outer wing section profile is twisted by  $5^\circ$  around the leading edge to reduce the aerodynamic loads and shift the onset of flow separation to higher angles of attack.

The SACCON wind tunnel model was designed to accommodate a belly sting mount for tests in the German-Dutch Low Speed Wing Tunnel (DNW-NWB) at DLR in Braunschweig. The sting, however, was not included in the commotional grid of this work.

A full-span grid was generated to perform CFD simulations in Cobalt and Kestrel flow solvers. This grid was generated in two steps. In the first step, the inviscid tetrahedral grid was generated using the ICEMCFD code. This grid was then used as a background grid by TRITET<sup>40,41</sup> which builds prism layers using an advancing front technique. TRITET rebuilds the viscous grid while respecting the size of the original inviscid grid from ICEMCFD. The grid is shown in Figure 4(a) and has 26,103,094 cells. Cobalt and Kestrel showed an average  $y+$  of 0.3 for a  $Re_c = 1.57$  million and  $M = 0.3$ . The predicted  $y+$  is shown in Fig. 5 for the top wing surface at  $M = 0.3$ .

For the USM3D flow solver, a full-span tetrahedral grid with 21,190,061 cells and 260,750 wing-surface triangles was generated for the clean-wing (i.e. no sting) DLR-F19 SACCON configuration shown in Figure 4 (b) using a developmental version of VGRID.<sup>36</sup> The clean-wing SACCON grid was produced from an identical wing surface definition (minus the belly sting) and VGRID source distribution as was used to create the SACCON grid G3.00 in Ref. 42. As described in Ref. 42, a thin-layer tetrahedral grid was generated with VGRID to meet requirements for cell-centered computations from the USM3D flow solver. A near-wall first-cell spacing was prescribed, based on flat-plate turbulent boundary layer theory, to achieve a tetrahedral cell centroid turbulent wall coordinate ( $y+$ ) of 0.5 at a longitudinal distance of  $0.5c$  for a  $Re_c = 1.5$  million, where  $c$  is the reference chord. Subsequent USM3D computations confirmed that an average first-cell  $y+ \approx 0.4$  was achieved. This “viscous” spacing distribution resulted in approximately 72 tetrahedral cells (24 nodes) across the boundary layer at the mid-chord of  $c$ .

## IV. Results and Discussion

### A. NACA0012 Airfoil

All airfoil simulations correspond to a Mach number of 0.6 and Reynolds number of 4.8 million. These conditions match with experimental conditions of AGARD test case CT2 (NACA 0012 airfoil).<sup>43</sup> All step response simulations are second-order accurate in time. Cobalt and Kestrel step simulations have five Newton subiterations as well. Step magnitudes are one degree for angle of attack step functions and one radian per second for the pitch rate step functions. For Kestrel, the pitch rate step magnitude is 10 rad/s.

The linear indicial responses of the airfoil with a unit step change of angle of attack are shown in Fig. 6 for all codes. In these figures, the angle-of-attack indicial functions per radian are plotted against non-dimensional time. Though, different grids were used and the codes have different numerical algorithms, CFD data of all codes match with each other very well. The normal force and pitch moment have a positive/negative peak at  $s = 0$  followed by a transient solution. The normal-force and pitch moment coefficients asymptotically reach the steady-state values after sufficient time has passed.

Figure. 7 shows the pitch-rate responses at  $\alpha = 0^\circ$ . Overall a good agreement was found between code data, particularly for the transient solutions. Cobalt and USM3D reach similar steady-state values. Normal force responses from ENSOLVE and Kestrel reach slightly different static values. Kestrel was found to be very sensitive to the pitch rate step magnitude. A converged solution in Kestrel was obtained for a step magnitude of 10 rad/s. The step magnitude in other codes is 1 rad/s. Note that in these simulations, the grid is pitching up but the angle of attack was held constant at zero degrees using the grid motion approach.

Linear aerodynamic models were created from responses shown in Figs. 6 and 7. The models were then used to predict aerodynamic responses to the AGARD CT2 pitch oscillation with available experimental

**Table 1. Description of the AGARD CT2 test conditions, NACA 0012 airfoil**

Test Conditions	Values
Mach Number, $M_\infty$	0.6
Mean Incidence, $\alpha_0$	$3.16^\circ$
Pitch Amplitude, $\alpha_A$	$4.59^\circ$
Reduced Frequency, $k$	0.0811
Reynolds Number, $Re$	$4.8 \times 10^6$

data. The AGARD CT2 test conditions are summarized in Table 1.

Figure 8 compares the model and full CFD data from all codes with experimental data of AGARD CT2 test case. Very good agreement is found between CFD and experimental data. The model predictions, on the other hand, match with each other and with CFD and experiments at small angles of attack. For large angles of attack, the linear models are off since the model formulation is valid in linear regimes.

To extend the validity range of models, angle-of-attack step responses were calculated at additional angles of attack. Figures 9 and 10 show these responses. Again, a good agreement was found between code predictions at small angles of attack. At higher angles (near stall angle), some code predictions do not match each other exactly. This may be due to grid resolution effects and differences in numerical algorithms on predictions at higher angles. Figures 9 and 10 show that the initial time solutions are invariant with angle of attack changes but the transient trend and steady state values change depending on the angle of attack.

The initial transient solutions can be explained based on the energy of acoustic wave systems created by the initial perturbation.<sup>44,45</sup> These waves depend on the flow compressibility and produce non-circulatory loads over the surface. As the response time progresses, the waves begin to move away from the vehicle and the circulatory forces become dominant. Therefore the final time solutions become different at different angles of attack.

A nonlinear ROM was created using these nonlinear responses and was used to predict aerodynamic responses of various pitch oscillation motions. The model predictions are compared with full CFD and available experimental data in Fig. 11. The figure shows that the non-linear ROM predictions agree well with each other and with full CFD data. Note that all these motions were generated within the  $\alpha$ -range of data used for model generation. A wide range of motions (combination of amplitude, mean angle, and frequency, or even plunging or ramp motions) can still be defined within this range where each motion takes much longer time (order of minutes or even hours) to be simulated in CFD than those predicted by the models (a few seconds).

## B. SACCON UCAV

SACCON simulations are performed at Mach numbers of 0.1, 0.3, and 0.5 and a Reynolds number of 1.57 million based on the reference chord of 0.48m. Static temperature was set to 288.15 K. The pressure and density are calculated from given Reynolds number and Mach number. The input angle of attack range has a range of  $-10^\circ$  to  $10^\circ$  for ROM creation. It is assumed that longitudinal forces/moments are symmetric with respect to the angle of attack and therefore the step responses are only calculated for positive step magnitudes.

Step magnitude is one degree for angle of attack step functions. For Kestrel and USM3D, the step magnitude used in angular rate simulations is 10 rad/s. For Cobalt the step magnitude is one radian per second. Second order accuracy in time was used for all step simulations. Cobalt and Kestrel again used five Newton subiterations. Time step was selected to set non-dimensional time ( $t^* = Vt/c$ ) to 0.01, where  $V$  and  $c$  denote freestream velocity and reference chord, respectively. Cobalt and Kestrel simulations were run on the Air Force Research Laboratory (AFRL) machines of Spirit and Thunder.

Figure 12 shows the indicial angle of attack responses of SACCON at zero angle of attack and Mach numbers of 0.1, 0.3, and 0.5. The predictions in Fig. 12 are shown for Cobalt, Kestrel, and USM3D flow solvers. A very good match is found between the predictions obtained from these codes. Similar to the airfoil case, normal force and pitch moment step responses of SACCON have an initial jump followed by a transient solution. The step responses will asymptotically approach the steady-state value after the transient

time interval. The initial jumps and the transient solutions are non-circulator forces because of the sudden acceleration of the grid, initially at rest.

In comparison to the NACA 0012 airfoil case, SACCON response simulations took much less time to reach the steady-state values. This is mainly due to three-dimensional effects on step responses. Ten thousands of time steps were run to complete the NACA 0012 airfoil step responses, while the SACCON step simulations were only run for 500 time steps. Figure 12 shows the effects of Mach number on the SACCON step functions as well. The initial jumps in solutions decrease as Mach number increases.

SACCON pitch rate responses were calculated using Cobalt, Kestrel, and USM3D flow solvers and are shown in Fig. 13. These simulations were started at zero degrees angle of attack and Mach numbers of 0.1, 0.3, and 0.5. The grid will suddenly pitch up with a rate of one radian per second in Cobalt. The pitch rates in Kestrel and USM3D are 10 rad/s. In all codes, the grid will move aft and upward to keep the angle of attack constant at zero degrees during pitch up motion. Figure 13 shows that again a good match was found between the simulation results of the codes. Pitch rate responses also show that an initial jump and a transient solution present due to the sudden grid acceleration. Again, the initial jumps decrease with increasing Mach number due to compressibility effects.

SACCON  $C_{N\alpha}$  and  $C_{m\alpha}$  responses were calculated at additional angles of attack and are shown in Fig. 14 as well. For the range of angles of attack considered in the plots ( $\alpha \leq 10^\circ$ ) the response solutions are almost similar. This confirms that the SACCON normal force and pitch moment coefficients are linear in this range of angles of attack.

The lateral responses of SACCON to a unit step change in the side slip angle are shown in Fig. 15 for Mach numbers of 0.1, 0.3, and 0.5 and zero degrees angle of attack. In these simulations, the solution starts from a steady-state condition at zero degrees side slip angle, and then initiates a lateral step motion such that the side slip angle is held constant to one degree and angle of attack is held constant to zero degrees for all  $t > 0$ . Likewise, for the lift and pitch moment, the initial peaks in lateral responses become smaller for compressible flow.

An investigation of the outlying correlation of USM3D relative to the Cobalt and Kestrel solutions in Figures 15-17 resulted in the discovery of a bug in computation of skin friction through the moving-grid path of USM3D. The pressure components of force and moment were confirmed to be in close agreement for all codes. This problem was exposed in Figures 15-17 because of a fortunate attribute that the lateral components of skin friction and pressure forces on the tailless SACCON configuration were of the same order of magnitude. The resolution to this problem is still underway, but its discovery demonstrates the tremendous benefit of multi-code collaborations

Figure 15 shows that while Cobalt and Kestrel data match each other, but USM3D predictions are off. The USM3D solutions were investigated and differences in the results can be related to a code issue found when USM3D is coupled with FD-CADRE, a generalized dynamic process control manager for coupling various plugins, e.g., flow solver, 6-DoF motion generator.

Typically, the angle of attack effects are negligible for the responses due to the angular rates at low to moderate angles of attacks. Figures 16 and 17 show the SACCON indicial functions with respect to roll and yaw rates. Again, a very good match was found between Cobalt and Kestrel predictions.

A model was created based on SACCON longitudinal step responses for prediction of SACCON pitching motions. These motions are forced oscillation that have zero mean angle of attack, four or eight degrees amplitude and motion frequencies of 3, 6, and 9 Hz. The time-marching CFD simulations of these motions were calculated using Cobalt. The computations start from a steady-state solution and then advance in time using second-order temporal accuracy. The ROM predictions were compared with CFD data in Figures 18 and 19. The comparisons between the created ROM with the time-marching solution shows good agreements for normal force and pitch moment and all solvers. Figures 18 and 19 show the lift curve would exhibit a clockwise hysteresis loop, but the pitch moment shows a counterclockwise loop. The loops will become thicker as the motion frequency increases.

## V. Conclusions

The convolution of aircraft responses to step inputs is considered as a powerful tool to take into account the time history effects on the aerodynamic coefficients. However, the calculation of step functions for compressible flow and three-dimensional geometries is challenging task. A grid motion approach was used in this work to calculate the response functions of a close gap NACA 0012 airfoil and the SACCON UCAV. A

surrogate model with these responses was then used to predict the aerodynamics of test cases during different pitching motions. To demonstrate the generalization capabilities of the grid motion approach for calculating step responses in CFD, the step functions were calculated with four different CFD flow solvers, namely Cobalt and Kestrel codes at USAFA, USM3D at LaRC, and ENSOLV at NLR. The model predictions were compared with CFD (full-order) and available experiments.

The results demonstrated that step functions can be easily calculated by CFD codes. Overall, the angle-of-attack and pitch rate responses were very similar for each solver particularly at small angles of attack. Discrepancies at higher angles were probably due to differences in grids and solver numerical algorithms. The step responses showed an initial jump as the grid begins to move. The initial jumps became smaller with increasing Mach number. All responses asymptotically reached a steady-state value. The results showed that much less time was required to reach the steady-state solutions for the UCAV geometry than two-dimensional airfoil. Finally, the model predictions matched the CFD data of different motions, all generated within the range of data used for model generation, very well.

## VI. Acknowledgements

Mehdi Ghoreyshi is supported by USAFA under contract FA70001320018; their financial support is gratefully acknowledged. The USAFA authors acknowledge the Department of Defense High Performance Computing Modernization Program (HPCMP), AFRL for providing computer time. The USAFA authors appreciate the support provided by the High Performance Computing Research Center at USAFA as well.

The NASA contributions were supported by the Technologies for Assuring Safe Aircraft Energy and Attitude State (TASEAS) work element under the NASA Airspace Operations and Safety Program, Airspace Technology Demonstration (ATD) project. The NASA computations were performed on the NASA Langley Research Center, Mid-Range k-cluster.

## References

- <sup>1</sup>Greenwell, D. J., "Difficulties in the Application of Stability Derivatives to the Maneuvering Aerodynamics of Combat Aircraft," *Proceedings of the 21st Congress of the International Council of the Aeronautical Sciences*, ICAS 1998-3.9.2, 1998.
- <sup>2</sup>Cebeci, T., *Numerical and Physical Aspects of Aerodynamic Flows IV*, Springer Berlin Heidelberg, 2013.
- <sup>3</sup>Schütte, A., Einarsson, G., Raichle, A., Schoning, B., Mönnich, W., and Forkert, T., "Numerical Simulation of Manoeuvring Aircraft by Aerodynamic, Flight Mechanics, and Structural Mechanics Coupling," *Journal of Aircraft*, Vol. 46, No. 1, 2009, pp. 53–64.
- <sup>4</sup>Ghoreyshi, M., Vallespin, D., Da Ronch, A., Badcock, K. J., Vos, J., and Hitzel, S., "Simulation of Aircraft Manoeuvres based on Computational Fluid Dynamics," AIAA Paper 2010–8239, August 2010.
- <sup>5</sup>Ghoreyshi, M., Jirasek, A., and Cummings, R. M., "CFD Modeling for Trajectory Predictions of a Generic Fighter Configuration," AIAA Paper 2011–6523, August 2011.
- <sup>6</sup>Stark, V. J. E., "Indicial Coefficients for a Cropped Delta Wing in Incompressible Flow," *Journal of Aircraft*, Vol. 23, No. 5, 1985, pp. 370–375.
- <sup>7</sup>Lisandrin, P., Carpentieri, G., and van Tooren, M., "Investigation over CFD-based Models for the Identification of Nonlinear Unsteady Aerodynamic Responses," *AIAA Journal*, Vol. 44, No. 9, 2006, pp. 2043–2050.
- <sup>8</sup>Leishman, J. G. and Nguyen, K. Q., "State-Space Representation of Unsteady Airfoil Behavior," *AIAA Journal*, Vol. 28, No. 5, 1989, pp. 836–844.
- <sup>9</sup>Tobak, M. and Schiff, L. B., "On the Formulation of the Aerodynamic Characteristics in Aircraft Dynamics," NASA TR R-456, 1976.
- <sup>10</sup>Ghoreyshi, M., Post, M. L., and Cummings, R. M., "CFD Calculation of Aerodynamic Indicial Functions for a Generic Fighter Configuration," *ITEA journal of Test and Evaluation*, Vol. 33, No. 6, 2012, pp. 348–364.
- <sup>11</sup>Ghoreyshi, M. and Cummings, R. M., "Unsteady Aerodynamics Modeling for Aircraft Maneuvers: a New Approach Using Time-Dependent Surrogate Modeling," *Journal of Aerospace Science and Technology*, Vol. 39, 2014, pp. 222 – 242.
- <sup>12</sup>Ghoreyshi, M., Cummings, R. M., DaRonch, A., and Badcock, K. J., "Transonic Aerodynamic Load Modeling of X-31 Aircraft Pitching Motions," *AIAA Journal*, Vol. 51, No. 10, 2013, pp. 2447–2464.
- <sup>13</sup>Wagner, H., "Über die Entstehung des dynamischen Auftriebes von Tragflügeln," *Zeitschrift für angewandte Mathematik und Mechanik*, Vol 1, Book 1, 1925, pp. 17–35.
- <sup>14</sup>Bisplinghoff, R. L. Ashley, H. and Halfman, R. L., *Aeroelasticity*, Dover Publications, Mineola, N.Y., 1996.
- <sup>15</sup>Ghoreyshi, M., Jirasek, A., and Cummings, R. M., "Computational Investigation into the Use of Response Functions for Aerodynamic Loads Modeling," *AIAA Journal*, Vol. 50, No. 6, 2012, pp. 1314–1327.
- <sup>16</sup>Ballhaus, W. F. and Goorjian, P. M., "Computation of Unsteady Transonic Flows by the Indicial Method," *AIAA Journal*, Vol. 16, No. 2, 1978, pp. 117–124.
- <sup>17</sup>Singh, R. and Baeder, J., "Direct Calculation of Three-Dimensional Indicial Lift Response Using Computational Fluid Dynamics," *Journal of Aircraft*, Vol. 34, No. 4, 1997, pp. 465–471.

- <sup>18</sup>Ghoreyshi, M. and Cummings, R. M., “Unsteady Aerodynamic Modeling of Aircraft Control Surfaces by Indicial Response Methods,” *AIAA Journal*, Vol. 52, No. 12, 2014, pp. 2683–2700.
- <sup>19</sup>Tobak, M., “On the Use of the Indicial Function Concept in the Analysis of Unsteady Motions of Wings and Wing-Tail Combinations,” NACA Report 1188, 1954.
- <sup>20</sup>Strang, W. Z., Tomaro, R. F., and Grismer, M. J., “The Defining Methods of Cobalt: A Parallel, Implicit, Unstructured Euler/Navier-Stokes Flow Solver,” AIAA Paper 1999-0786, 1999.
- <sup>21</sup>Gottlieb, J. J. and Groth, C. P. T., “Assessment of Riemann Solvers For Unsteady One-dimensional Inviscid Flows of Perfect Gasses,” *Journal of Fluids and Structure*, Vol. 78, No. 2, 1998, pp. 437–458.
- <sup>22</sup>Tomaro, R. F., Strang, W. Z., and Sankar, L. N., “An Implicit Algorithm For Solving Time Dependent Flows on Unstructured Grids,” AIAA Paper 1997-0333, 1997.
- <sup>23</sup>Spalart, P. R. and Allmaras, S. R., “A One Equation Turbulence Model for Aerodynamic Flows,” AIAA Paper 1992-0439, January 1992.
- <sup>24</sup>Wilcox, D. C., “Reassessment of the Scale Determining Equation for Advanced Turbulence Models,” *AIAA Journal*, Vol. 26, November, 1988, pp. 1299–1310.
- <sup>25</sup>Menter, F., “Eddy Viscosity Transport Equations and Their Relation to the  $k - \varepsilon$  Model,” *ASME Journal of Fluids Engineering*, Vol. 119, 1997, pp. 876–884.
- <sup>26</sup>Frink, N. T., “Tetrahedral Unstructured Navier-Stokes Method for Turbulent Flows,” *AIAA Journal*, Vol. 36, No. 11, 1998, pp. 1975–1982.
- <sup>27</sup>Frink, N. T., “A Flexible System for Analysis of Bodies in Relative Motion,” AIAA Paper 2005-5120, June 2005.
- <sup>28</sup>Pandya, M. J., Frink, N. T., Abdol-Hamid, K. S., Samareh, J. A., Parlette, E. B., and Taft, J. R., “Enhancements to TetrUSS for NASA Constellation Program,” *Journal of Spacecraft and Rockets*, Vol. 49, No. 4, 2012, pp. 617–631.
- <sup>29</sup>“ENFLOW: A Computer Code System for Accurate Simulation of Three-Dimensional Flows,” URL: <http://www.nlr.nl/documents/flyers/f222-01.pdf> [cited 01 June 2015].
- <sup>30</sup>Dol, H. S., Kok, J. C., and Oskam, B., “Turbulence Modeling for Leading-Edge Vortex Flows,” AIAA Paper 2002-0843, 2002.
- <sup>31</sup>Dol, H. S., Kok, J. C., Oskam, B., and van der Ven, H., “Extra-Large Eddy Simulation of Massively Separated Flows,” NLR-TP- 2003-200, 2003.
- <sup>32</sup>Roth, G. L., Morton, S. A., and Brooks, G. P., “Integrating CREATE-AV Products DaVinci and Kestrel: Experiences and Lessons Learned,” AIAA Paper 2012-1063, January 2012.
- <sup>33</sup>Morton, S. A., McDaniel, D. R., Sears, D. R., Tillman, B., and Tuckey, T. R., “Kestrel: A Fixed Wing Virtual Aircraft Product of the CREATE Program,” AIAA Paper 2009-0338, January 2009.
- <sup>34</sup>Godunov, S. K., “A Difference Scheme for Numerical Computation of Discontinuous Solution of Hydrodynamic Equations,” *Sbornik Mathematics*, Vol. 47, 1959, pp. 271–306.
- <sup>35</sup>Grismer, M. J., Strang, W. Z., Tomaro, R. F., and Witzeman, F. C., “Cobalt: A Parallel, Implicit, Unstructured Euler/Navier-Stokes Solver,” *Advanced Engineering Software*, Vol. 29, No. 3-6, 1998, pp. 365–373.
- <sup>36</sup>Pirzadeh, S. Z., “Advanced Unstructured Grid Generation for Complex Aerodynamic Applications,” *AIAA Journal*, Vol. 48, No. 5, 2010, pp. 904–915.
- <sup>37</sup>Spekreijse, S. P. and Nijhuis, G. H., “User Guide of Endomo Version 2.60, A Graphical Interactive Domain Decomposer For Multi-Block Domain Decomposition of Arbitrary Flow Domains,” NLR-CR-98436, 1999.
- <sup>38</sup>Spekreijse, S. P. and Nijhuis, G. H., “User Guide of Engrid, Version 4.20, A Graphical Interactive Grid Generator For Arbitrary Multi-Block Domains,” NLR-CR-98436, 1998.
- <sup>39</sup>Cummings, R. M. and Schütte, A., “An Integrated Computational/Experimental Approach to UCAV Stability & Control Estimation: Overview of NATO RTO AVT-161,” AIAA Paper 2010-4392, June-July 2010.
- <sup>40</sup>Tyssel, L., “Hybrid Grid Generation for Complex 3D Geometries,” Proceedings of the 7th International Conference on Numerical Grid Generation in Computational Field Simulation, 2000, pp. 337–346.
- <sup>41</sup>Tyssel, L., “The TRITET Grid Generation System,” International Society of Grid Generation (ISGG),” Proceedings of the 10th International Conference on Numerical Grid Generation in Computational Field Simulations, 2000.
- <sup>42</sup>Frink, N. T., “Stability and Control CFD Investigations of a Generic 53-deg Swept UCAV Configuration,” AIAA Paper 2014-2133, June 2014.
- <sup>43</sup>Landon, R. H., “NACA 0012. Oscillating and Transient Pitching,” In Compendium of Unsteady Aerodynamic Measurements, AGARD-R-702, Data Set 3, August 1982.
- <sup>44</sup>Lomax, H., “Indicial Aerodynamics,” AGARD Manual of Aeroelasticity, Part II, 1960, Chapter 6.
- <sup>45</sup>Leishman, J., “Indicial Lift Approximations for Two-Dimensional Subsonic Flow as Obtained from Oscillatory Measurements,” *Journal of Aircraft*, Vol. 30, No. 3, 1993, pp. 340–351.

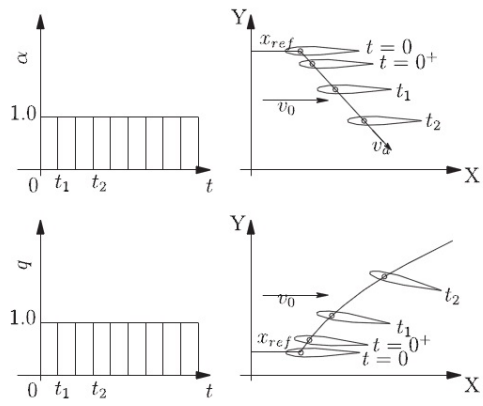


Figure 1. The grid motion for modeling a step change in angle of attack and pitch rate

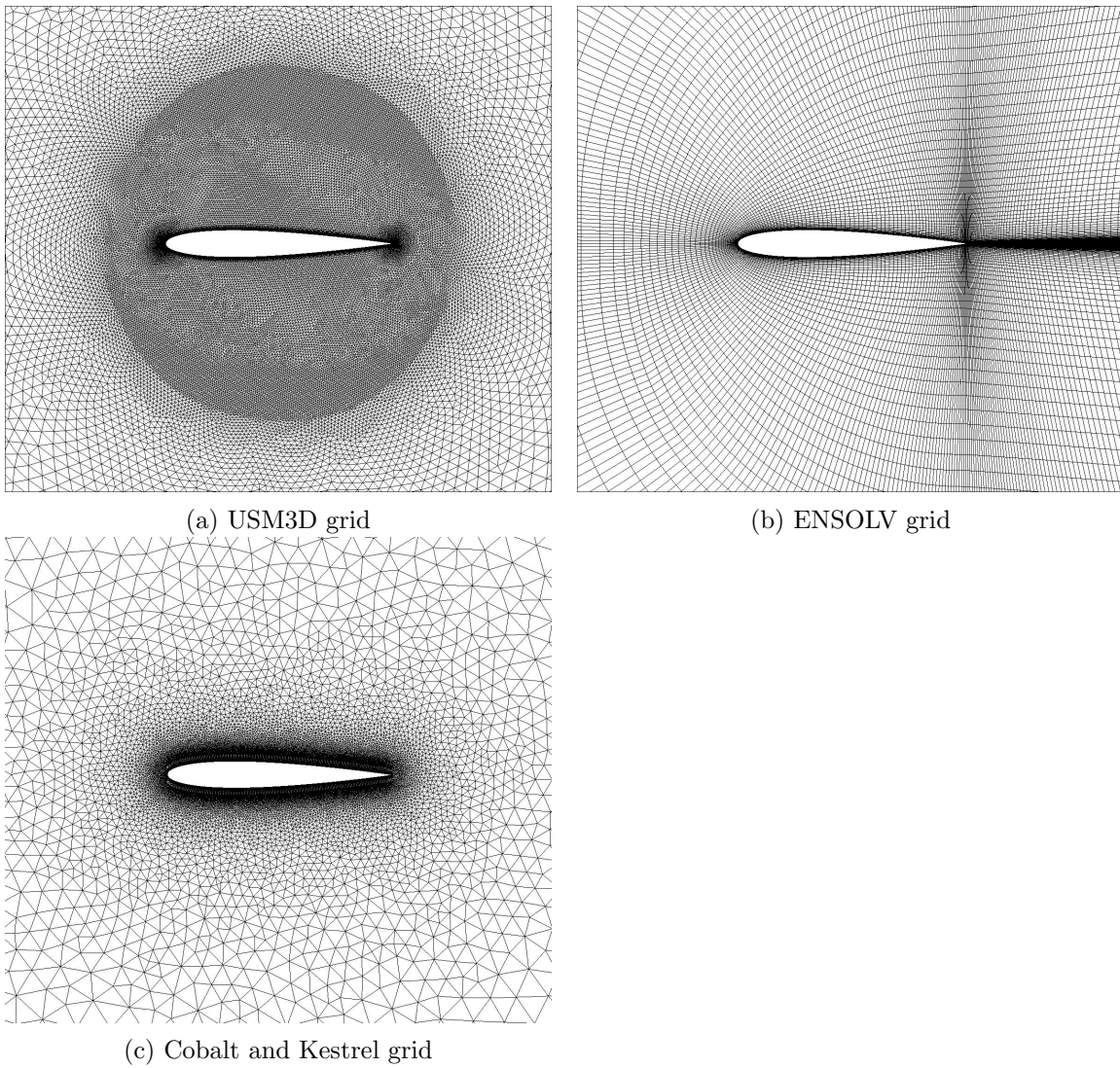


Figure 2. NACA0012 airfoil grids.

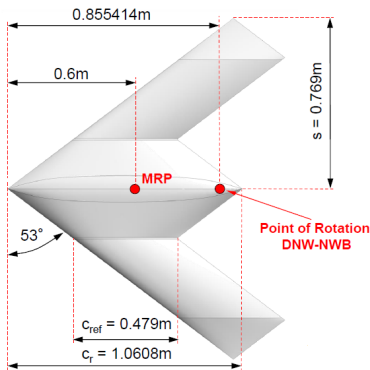


Figure 3. The SACCON geometry.<sup>39</sup>

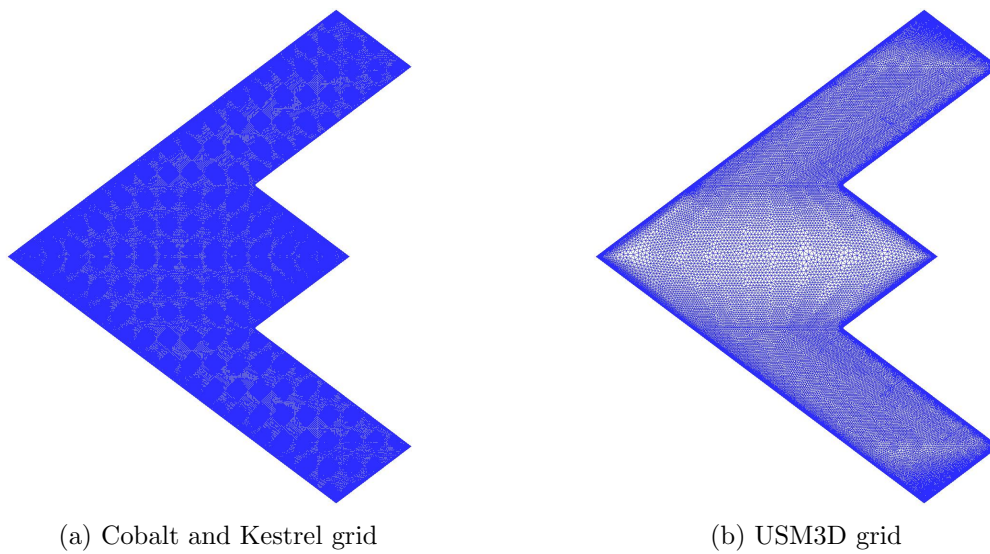


Figure 4. SACCON surface grids.

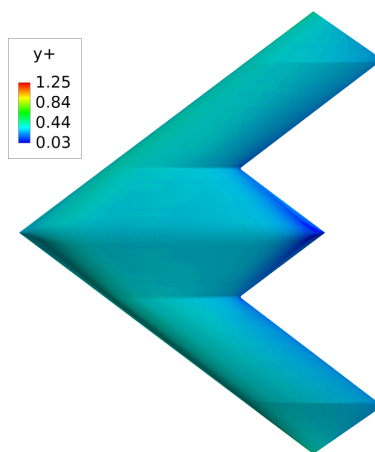


Figure 5.  $y^+$  plot of the SACCON grid used in Cobalt/Kestrel.

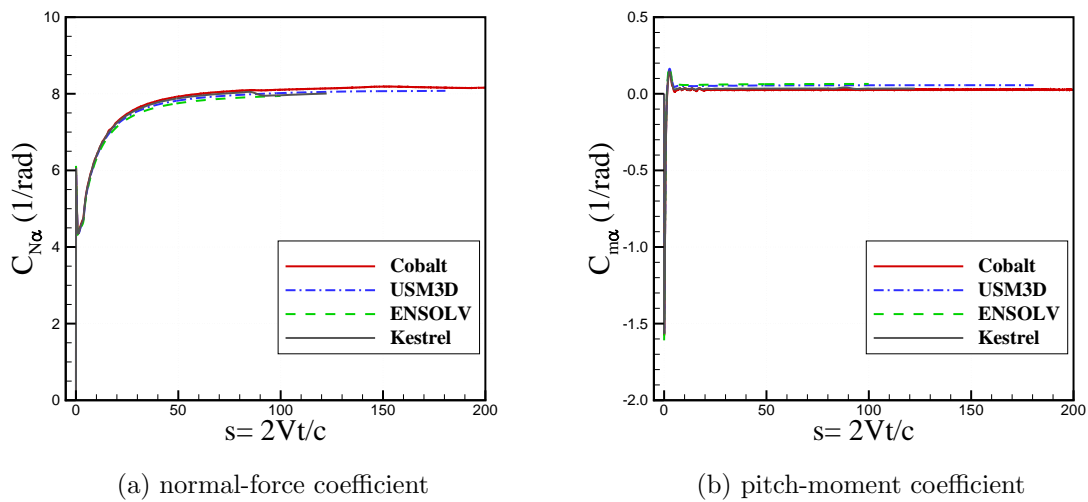


Figure 6. Linear angle-of-attack indicial responses. NACA0012,  $\alpha = 0^\circ$ , and  $M = 0.6$ .

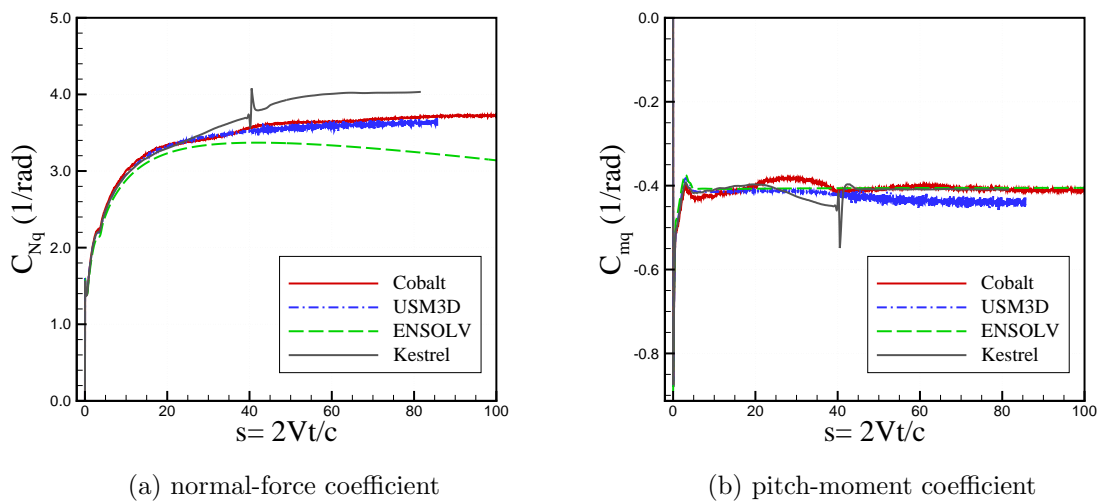
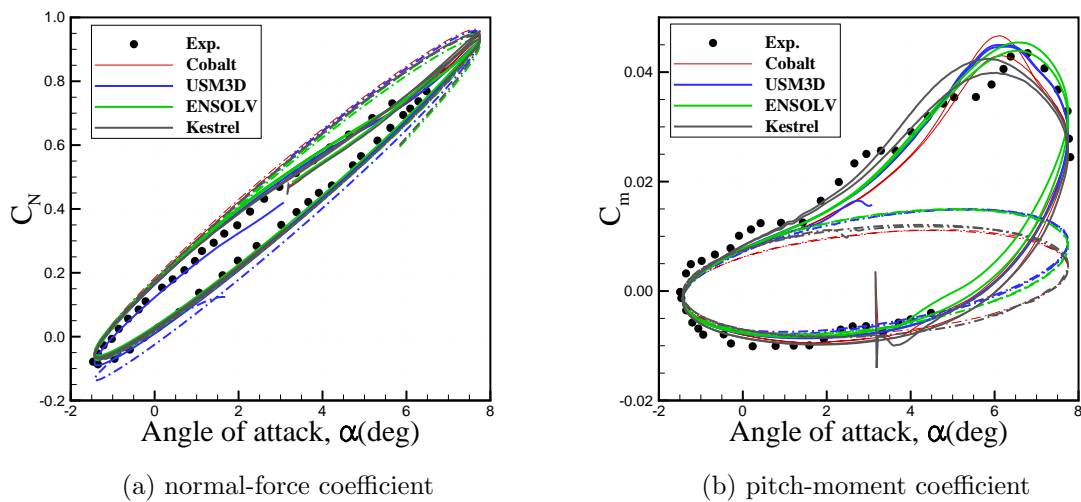


Figure 7. Linear pitch-rate indicial responses. NACA0012,  $\alpha = 0^\circ$ , and  $M = 0.6$ .



**Figure 8. Multi-code comparison of linear ROM (dashed lines) and full CFD (solid lines) with AGARD CT2 NACA0012 experimental data undergoing sinusoidal pitch oscillation,  $\alpha = 3.16^\circ + 4.59^\circ \sin(\omega t)$ ,  $f = 10.54$  Hz.,  $M = 0.6$ .**

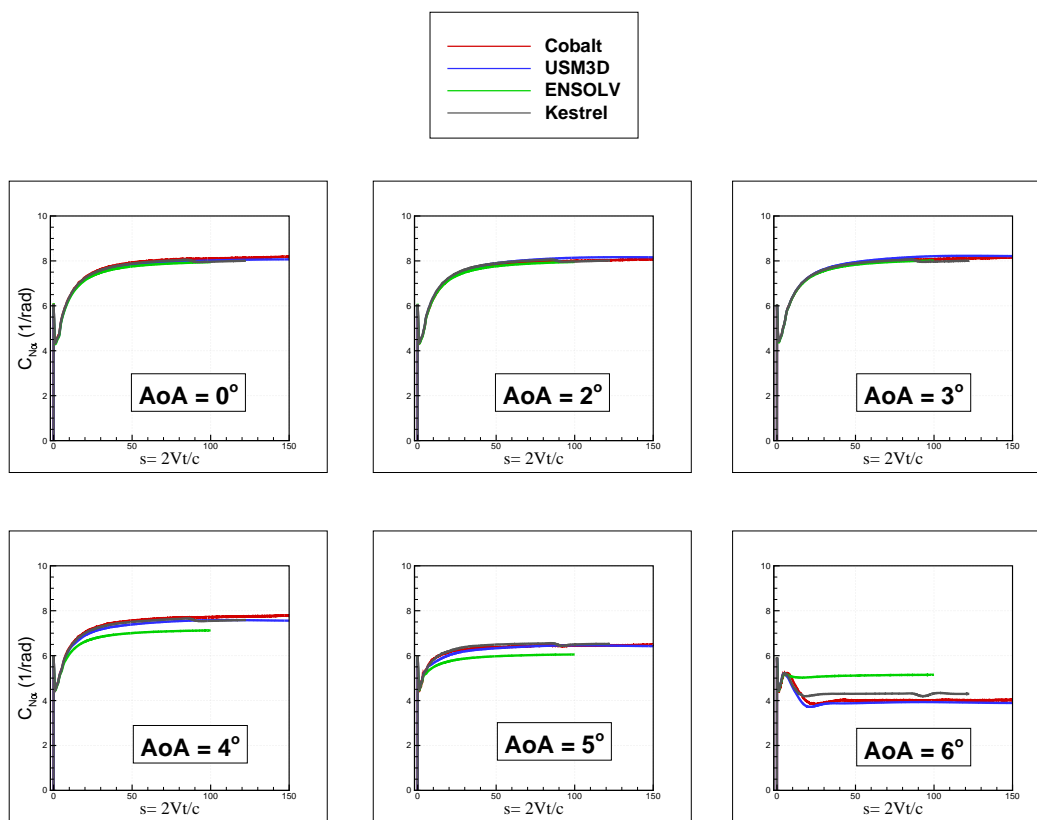


Figure 9. Nonlinear normal force angle-of-attack indicial responses. NACA0012 and  $M = 0.6$ .

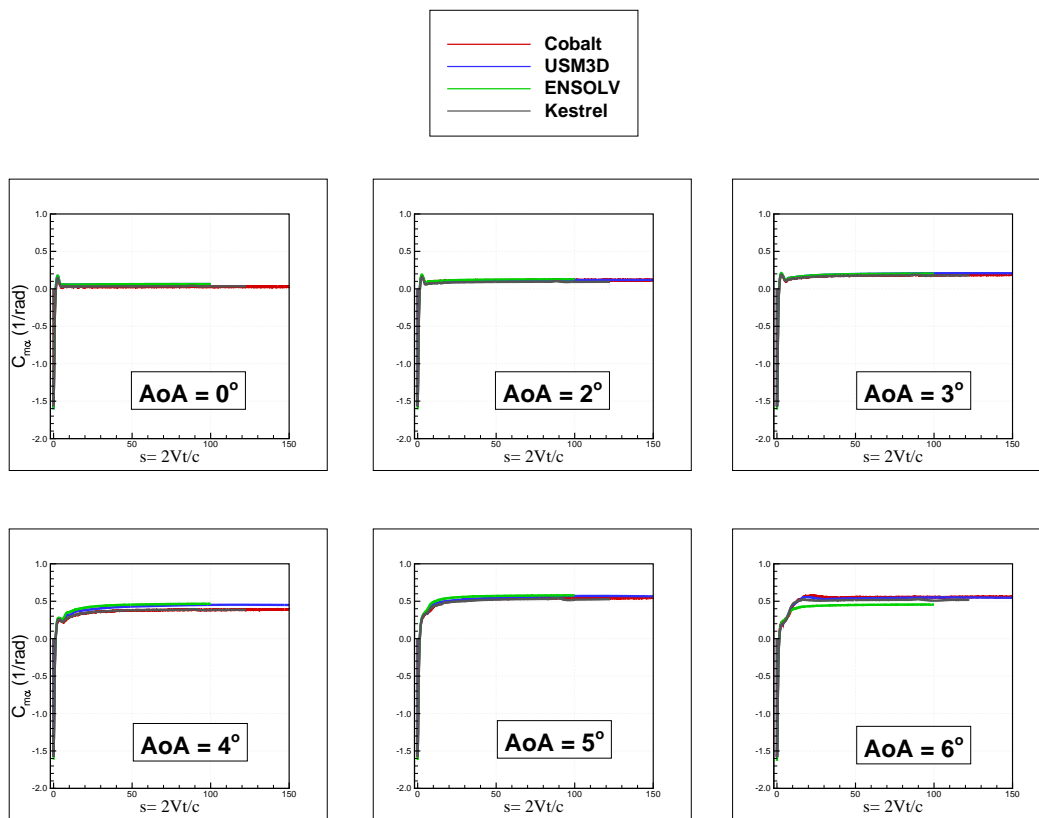
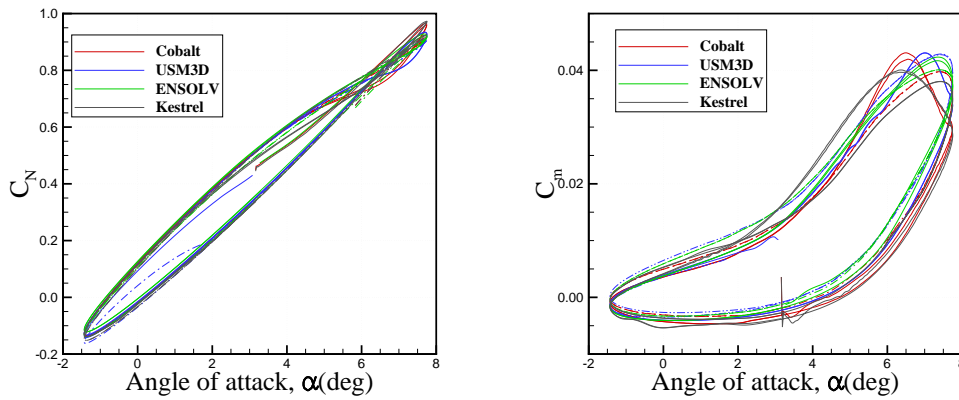
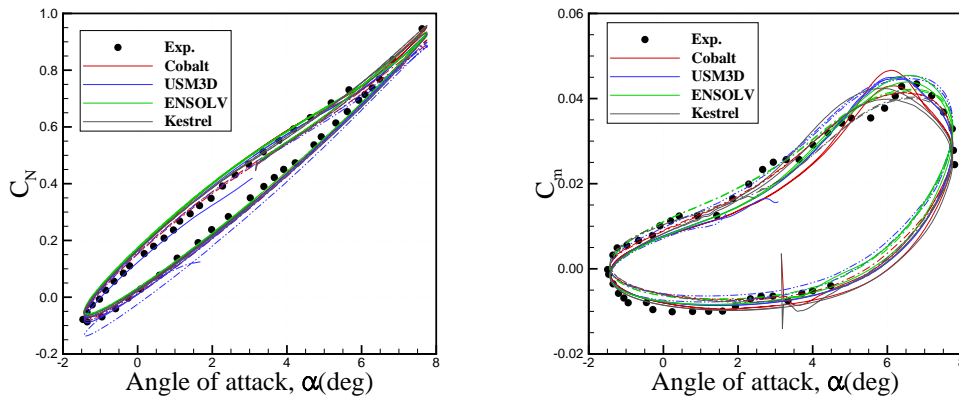


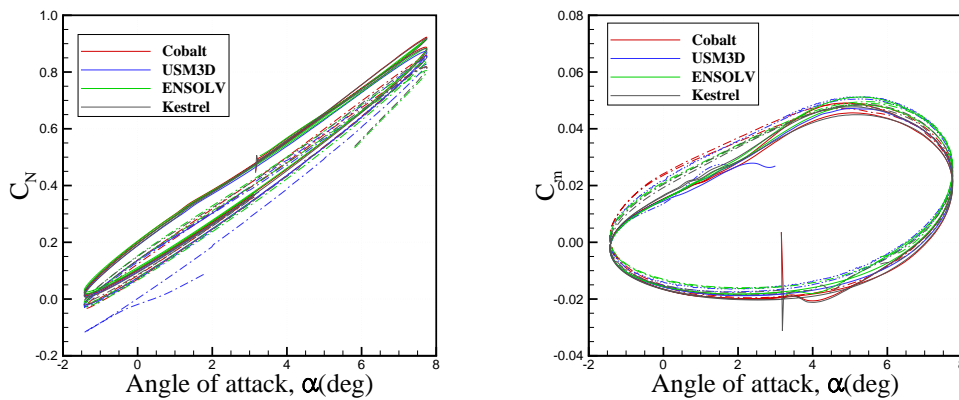
Figure 10. Nonlinear pitch moment angle-of-attack indicial responses. NACA0012 and  $M = 0.6$ .



(a)  $\alpha = 3.16^\circ + 4.59^\circ \sin(\omega t)$ ,  $f = 2.63$  Hz.



(a)  $\alpha = 3.16^\circ + 4.59^\circ \sin(\omega t)$ ,  $f = 5.27$  Hz.



(a)  $\alpha = 3.16^\circ + 4.59^\circ \sin(\omega t)$ ,  $f = 10.54$  Hz.

**Figure 11. Multi-code comparisons of aerodynamic modeling using nonlinear response functions. NACA0012,  $M = 0.6$ . (Solid and dashed lines correspond to full-CFD and ROM data, respectively.)**

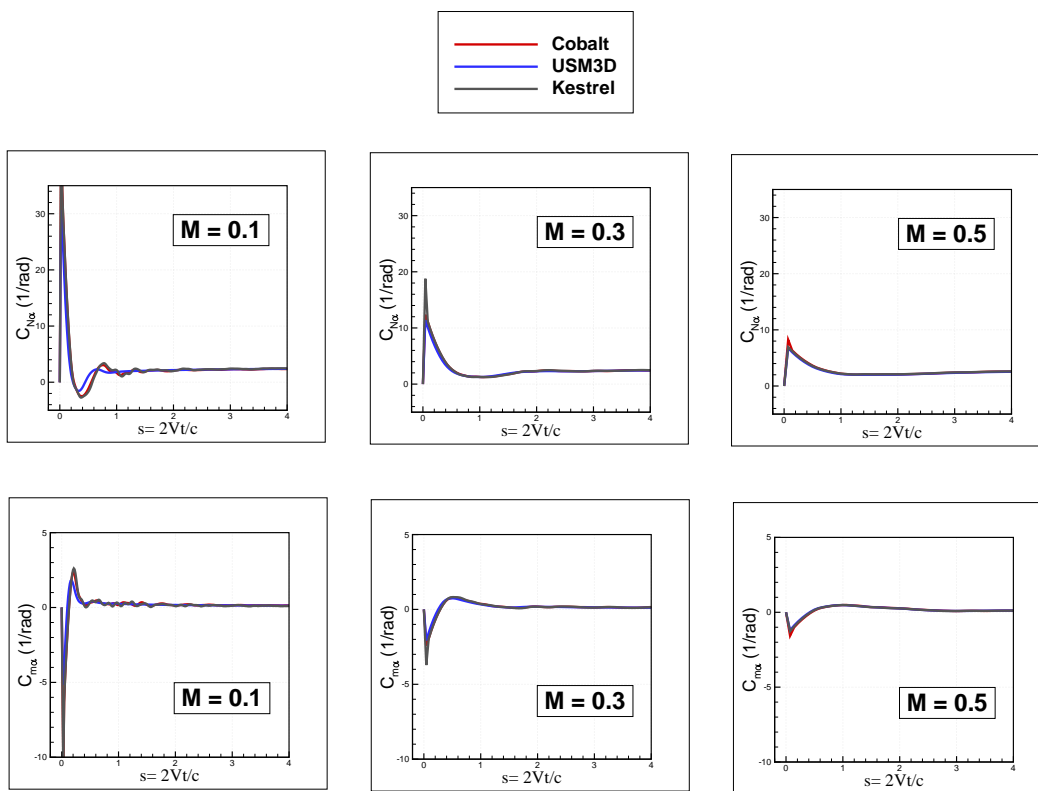


**Figure 12. Linear angle-of-attack indicial responses for normal force and pitching moment at  $M = 0.1, 0.3,$  and  $0.5$ . SACCON,  $\alpha = 0^\circ$ .**

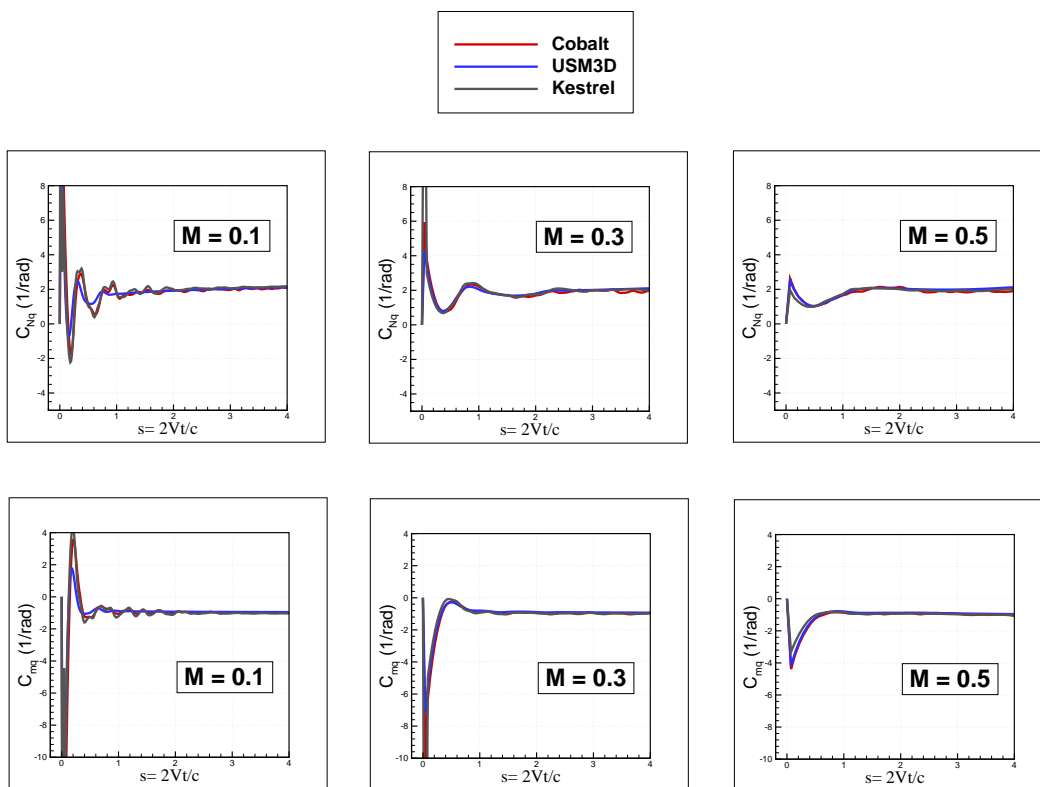


**Figure 13.** Linear pitch-rate indicial responses for normal force and pitching moment at  $M = 0.1, 0.3,$  and  $0.5$ . SACCON,  $\alpha = 0^\circ$ .

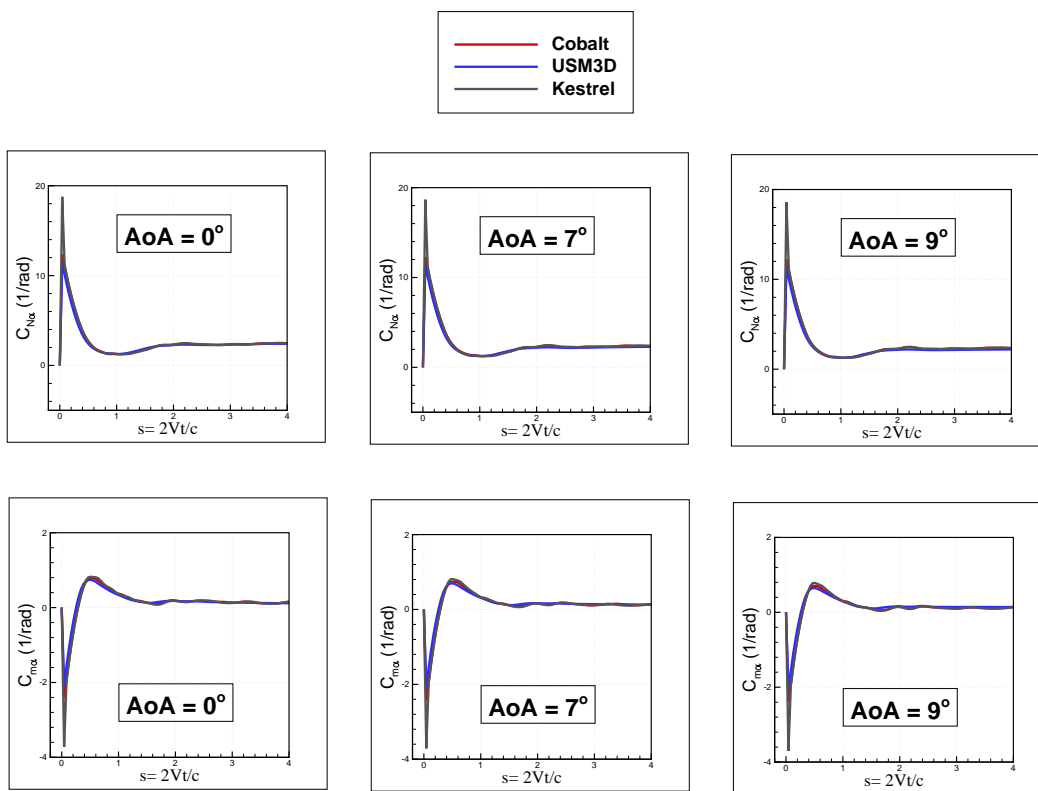


Figure 14. Nonlinear angle-of-attack indicial responses for normal force and pitching moment. SACCON,  $M = 0.3$ .

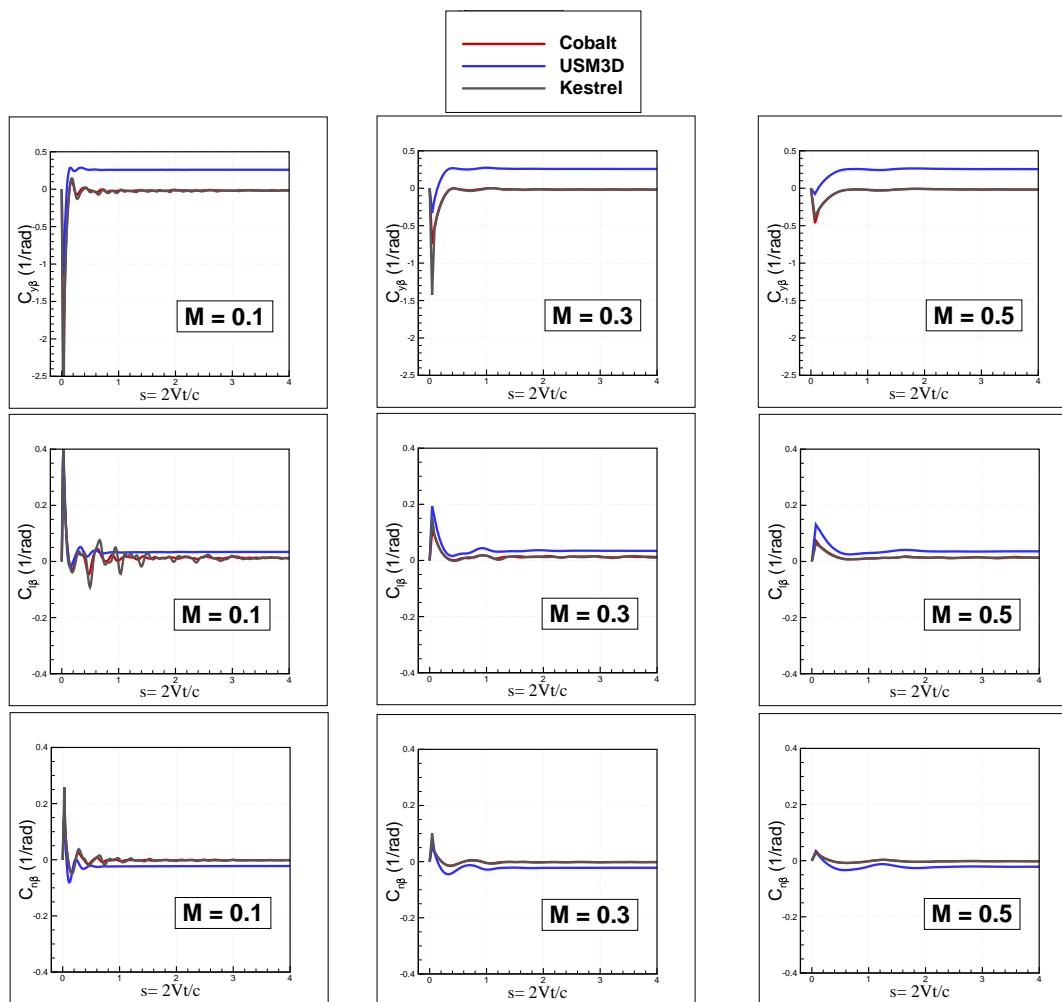
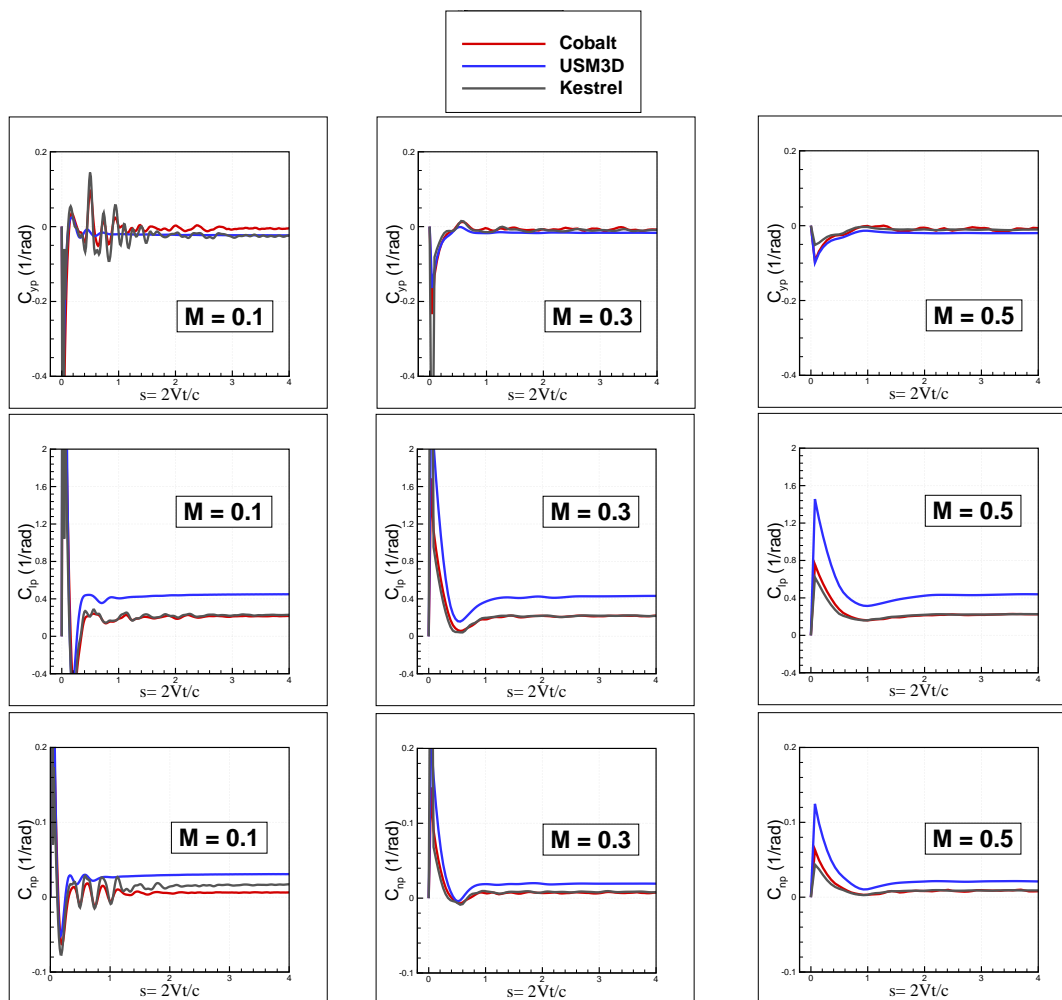


Figure 15. Side-slip indicial responses for side force, rolling and yawing moment at  $M = 0.1, 0.3,$  and  $0.5$ . SACCON,  $\alpha = 0^\circ$ .



**Figure 16.** Roll-rate indicial responses for side force, rolling and yawing moment at  $M = 0.1, 0.3,$  and  $0.5$ . SACCON,  $\alpha = 0^\circ$ .

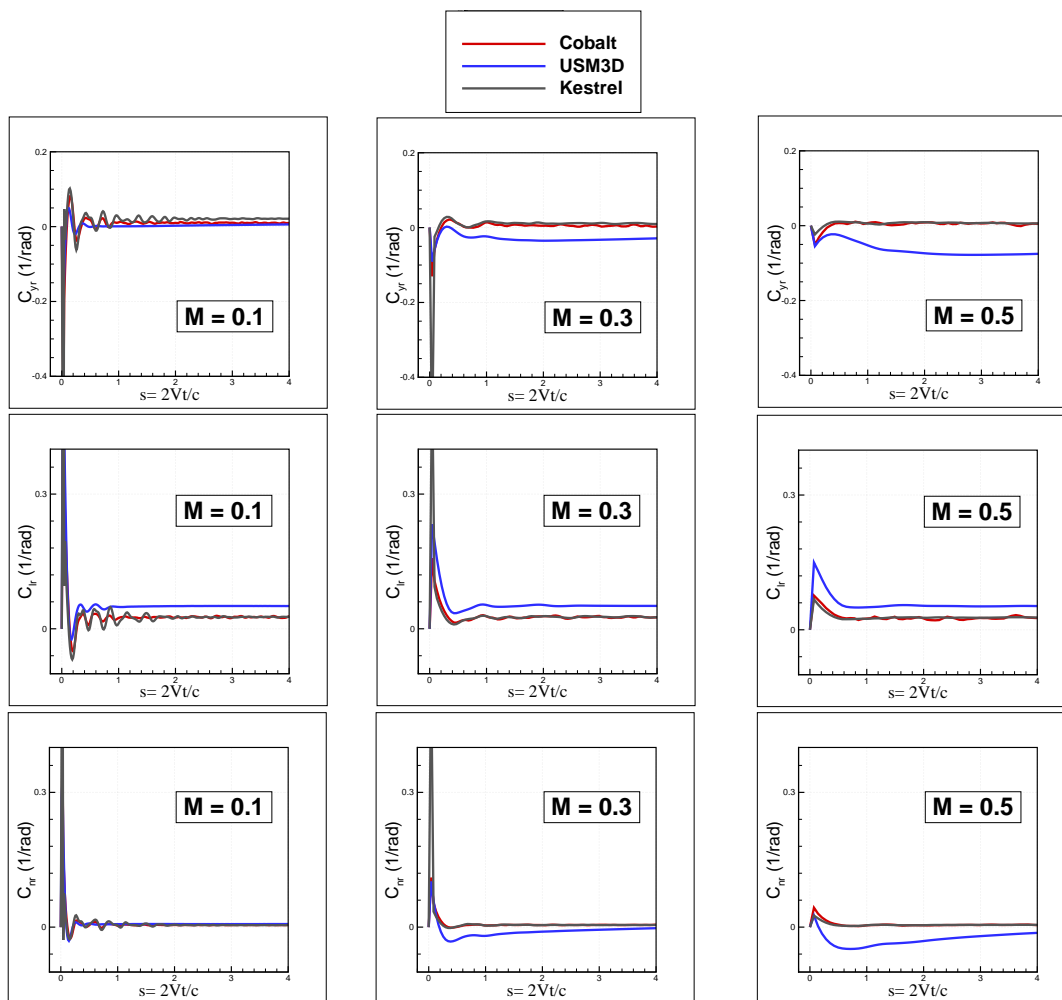
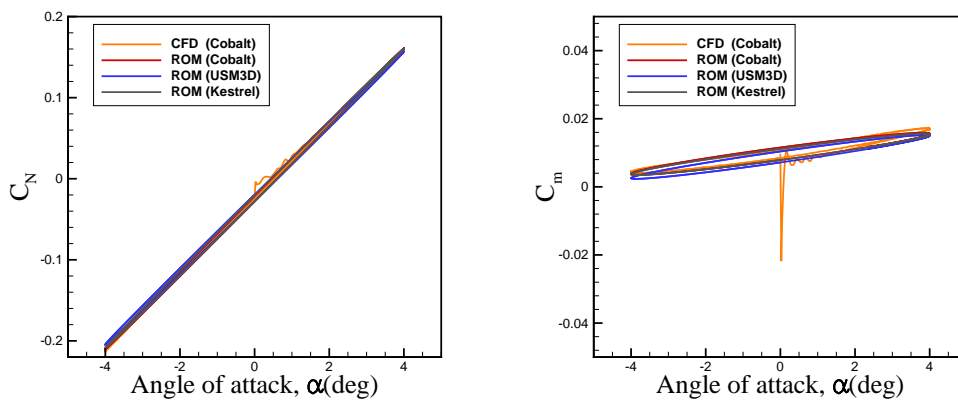
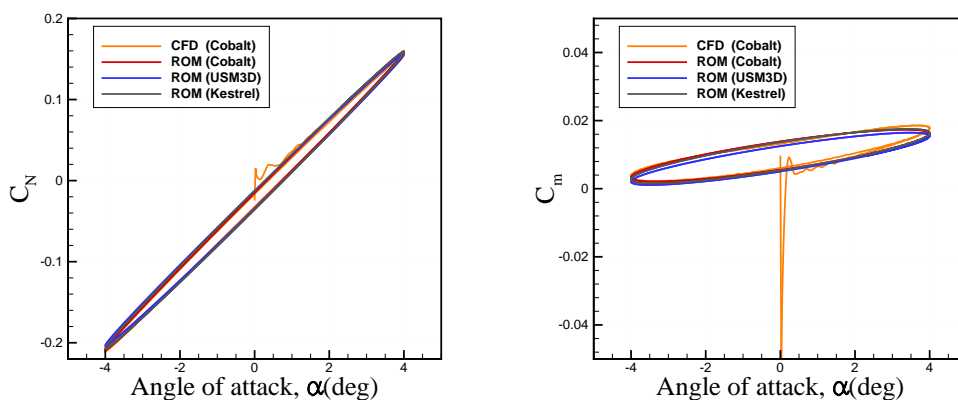


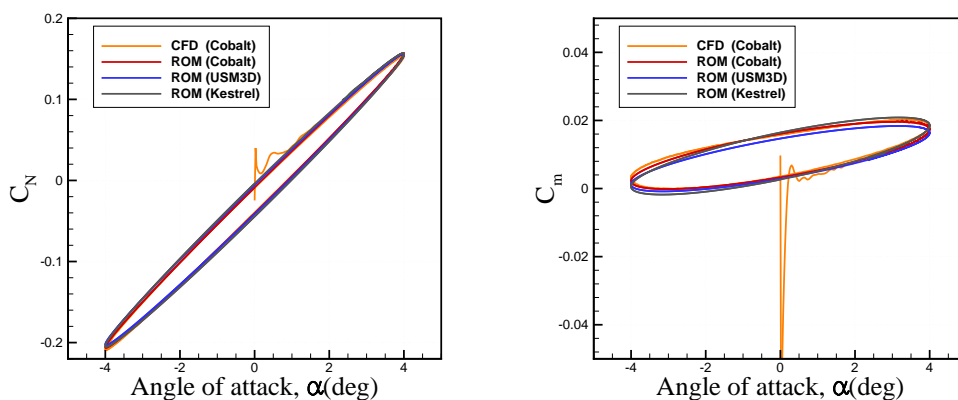
Figure 17. . Yaw-rate indicial responses for side force, rolling and yawing moment at  $M = 0.1, 0.3$ , and  $0.5$ . SACCON,  $\alpha = 0^\circ$ .



(a)  $\alpha = 4.0^\circ \sin(\omega t)$ ,  $f = 3$  Hz.

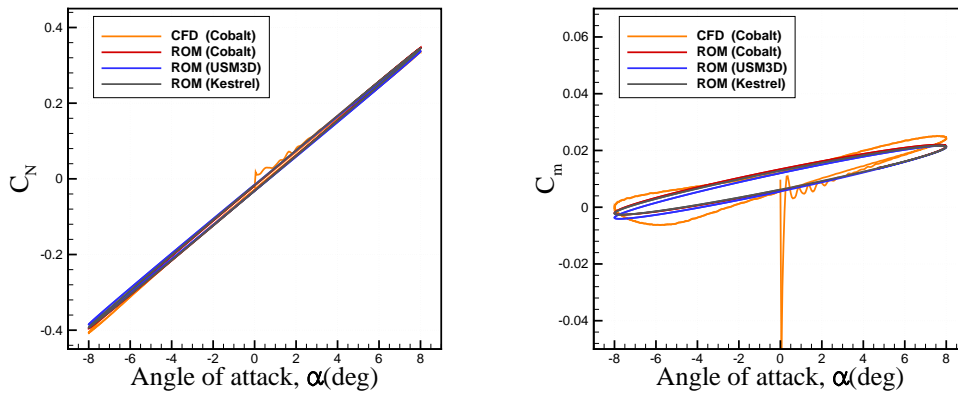


(b)  $\alpha = 4.0^\circ \sin(\omega t)$ ,  $f = 6$  Hz.

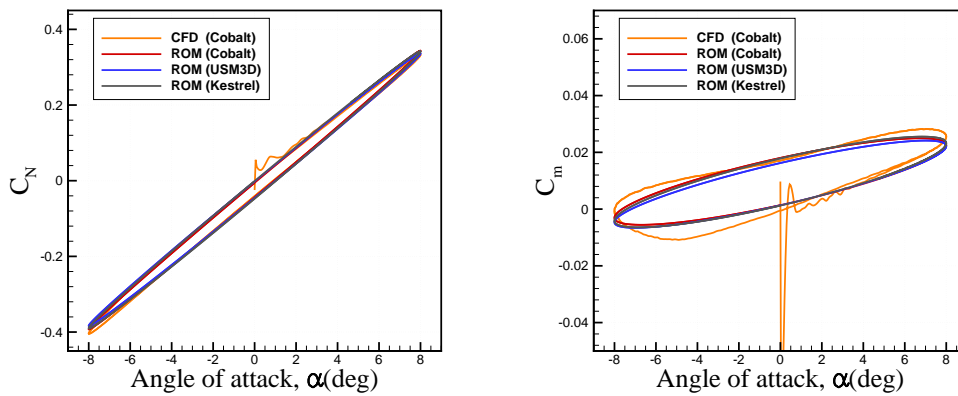


(c)  $\alpha = 4.0^\circ \sin(\omega t)$ ,  $f = 9$  Hz.

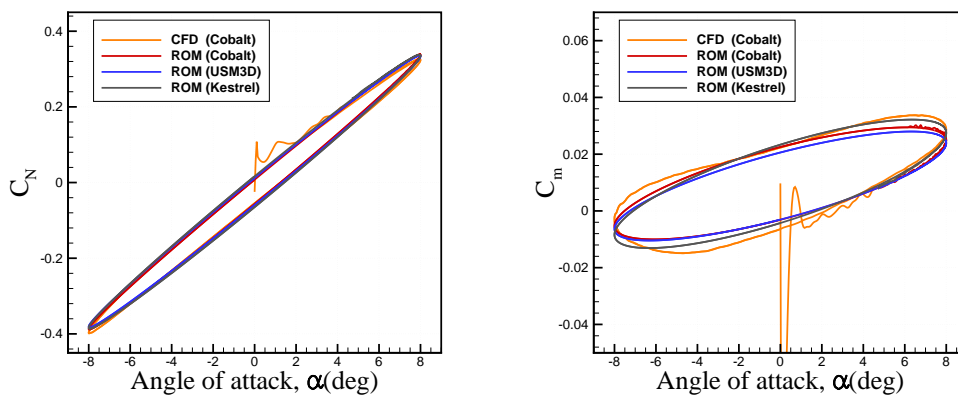
Figure 18. Multi-code comparison of ROM and full Cobalt CFD with SACCON motions with four degrees amplitude and zero mean pitch angle at  $M = 0.3$ .



(a)  $\alpha = 8.0^\circ \sin(\omega t)$ ,  $f = 3$  Hz.



(b)  $\alpha = 8.0^\circ \sin(\omega t)$ ,  $f = 6$  Hz.



(c)  $\alpha = 8.0^\circ \sin(\omega t)$ ,  $f = 9$  Hz.

Figure 19. Multi-code comparison of ROM and full Cobalt CFD with SACCON motions with eight degrees amplitude and zero mean pitch angle at  $M = 0.3$ .